Article

Nitrogen-Doped Activated Hollow Carbon Nanofibers with Controlled Hierarchical Pore Structures for High-Performance, Binder-Free, Flexible Supercapacitor Electrodes

TaeGyeong Lim, Bong Hyun Seo, Seo Ju Kim, Seungwoo Han, Wonyoung Lee, and Ji Won Suk*

Cite This: *ACS Omega* 2024, 9, 8247–8254

Read Online

ACCESS | Metrics & More | Article Recommendations | SI Supporting Information

ABSTRACT: Carbon nanofibers (CNFs) are a fascinating electrode material for energy storage devices due to their one-dimensionality, interconnected networks, and chemical stability. However, a relatively low specific surface area of CNFs hinders their use as supercapacitor electrodes. Here, nitrogen-doped hollow CNFs with hierarchical pore structures are prepared via electrospinning of core–shell polymer nanofibers and subsequent carbonization and activation under an ammonia atmosphere. Hierarchical pore structures with micro-, meso-, and macropores are controlled by an ammonia etching effect during the carbonization of polymer nanofibers. In addition, a hollow structure in CNFs is obtained by thermal decomposition of the core polymer during the carbonization/activation. The nitrogen-doped activated hollow CNFs (ahCNFs) exhibited an exceptionally high specific surface area of 3618 m^2/g with increased mesopores. Thus, a symmetric supercapacitor using ahCNFs electrodes with a 6 M KOH aqueous electrolyte provides a high specific capacitance of 208 F/g at a current density of 1 A/g, a high energy density of 7.22 W h/kg at a power density of 502 W/kg, a good rate capability, and cyclic stability. Moreover, the freestanding ahCNFs are used for flexible supercapacitor electrodes without any binder. This work demonstrates the great potential of highly porous ahCNFs for high-performance energy storage devices.
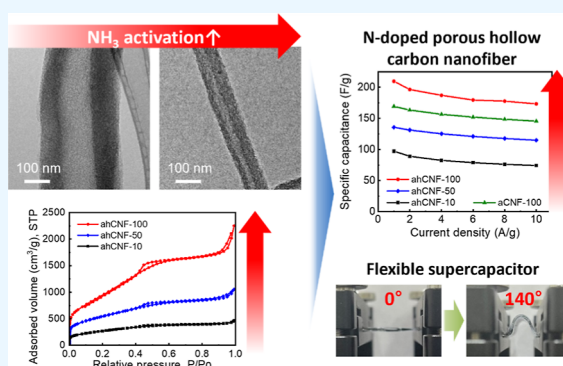
1. INTRODUCTION

The demand for high-performance and environment-friendly energy storage devices is increasing due to continuous and rapid developments in renewable energy resources, portable electronic devices, and electric vehicles.[1−3] Supercapacitors are considered promising energy storage devices owing to their high power density, high charge/discharge rate, long cycle life, low maintenance cost, and wide operating temperatures.[4,5] Supercapacitors are generally classified to electrical double-layer capacitors (EDLCs) by reversible electrostatic adsorption/desorption of electrolyte ions and pseudocapacitors by reversible faradaic redox reactions according to charge storage mechanisms.[6,7] EDLCs are used as commercial supercapacitors due to their low cost and great stability, while pseudocapacitors have poor cycle stability and require more expensive electrode materials such as RuO_2 and IrO_2.[8,9] However, the low energy density of EDLCs hampers their wide industrial applications.[10] Therefore, research on developing electrode materials with high energy density and power density is still a significant challenge.[11]

The electrochemical performance of EDLC electrodes depends on their surface area and pore size distributions.[12] Therefore, porous carbon materials have been intensively investigated as the electrode material of EDLCs due to their outstanding specific surface area (SSA), controllable porosity, and good electrical conductivity.[13,14] Among various carbon materials, carbon nanofibers (CNFs) possess excellent electrical conductivity, chemical stability, and one-dimensional geometry that is useful for ion diffusion.[15−19] CNFs can be synthesized using electrospinning and subsequent carbonization, which is a scalable manufacturing method to tune the morphology and chemical functionality of the nanofibers.[20−24]

In addition, SSAs of CNFs have been increased and controlled by using various approaches. Chemical activation typically using KOH has been widely applied for carbon nanomaterials to obtain micro- and mesoporous structures with high SSAs.[25−29] However, corrosive chemical agents are added to CNFs for the activation process at high temperatures and careful washing is required after the process.[30,31] Heat treatments conducted in an ammonia (NH_3) gas atmosphere have been explored as an alternative method for etching and

activating CNFs.[5,32,33] This straightforward and efficient process not only creates micro- and mesopores on the surfaces of CNFs but also introduces nitrogen-containing functional groups with pseudocapacitive behaviors and improved electrical conductivity.[5] Therefore, it has great potential as a facile synthesis method for porous CNFs used in high-performance supercapacitor electrodes. However, understanding the pore structures and nitrogen doping of CNFs through NH$_3$-based heat treatments has remained elusive for supercapacitor applications until now.

Incorporating sacrificial materials during polymer fiber synthesis offers an alternative approach to control the pore structures and construct the desired morphology of CNFs.[34] However, the sacrificial materials need to be completely removed by additional thermal or chemical treatments.[35] For example, water-soluble polyvinylpyrrolidone (PVP) has been introduced in CNFs as a soft template and subsequently removed by washing them with water.[36,37] Hard templates such as SiO$_2$ have been used in fabricating porous CNFs with the help of chemical etching of those templates using strong acid or base solutions.[38,39] Poly(methyl methacrylate) (PMMA) is an alternative template material that can be thermally decomposed to create pore structures. Therefore, by introducing PMMA into a CNF precursor polymer such as polyacrylonitrile (PAN), porous CNFs can be obtained during the carbonization step without any additional processing.[40]

In this work, we combined the electrospinning of PMMA/PAN core−shell nanofibers with a one-step NH$_3$-based carbonization/activation process to synthesize nitrogen-doped activated hollow CNFs (ahCNFs). While the thermal decomposition of the PMMA core created hollow CNFs, heat treatment under the NH$_3$ atmosphere led to the activation of CNFs during the simultaneous carbonization process. The effects of NH$_3$ gas on the structural, chemical, and electrochemical properties of CNFs were systematically investigated by controlling the NH$_3$ concentration. As a result, the ahCNF synthesized under an optimal NH$_3$ concentration exhibited an exceptionally high SSA of 3618 m^2/g. Therefore, the ahCNF sheet with hierarchical pore structures provided excellent electrochemical performances for a symmetric two-electrode supercapacitor with a KOH electrolyte. In addition, a flexible supercapacitor with high durability was demonstrated using free-standing, binder-free ahCNF electrodes.

2. EXPERIMENTAL METHODS

2.1. Synthesis of Activated Hollow Carbon Nanofibers.
To prepare polymer solutions for the electrospinning of core and shell parts, PAN (12 wt %, M_w = 150,000, Merck) and PMMA (15 wt %, M_w = 120,000, Merck) were separately dissolved in N,N-dimethylformamide (DMF, Merck) by stirring overnight at room temperature. The solutions were electrospun using a coaxial needle (25G−16G for the core−shell parts, NanoNC) with an applied voltage of 20 kV. The flow rates were set to 1 and 2 mL/h for the core and shell parts, respectively. The PMMA/PAN core−shell nanofiber sheet was collected on aluminum foil attached to a rotating drum (a rotating speed of 600 rpm and a distance from the nozzle tip of 17 cm). The polymer nanofiber sheets were heated to 280 °C and stabilized in air for 2 h. The temperature was raised to 1050 °C and kept for 1 h with an Ar flow rate of 100 mL/min for carbonization. NH$_3$ was introduced with flow rates of 10, 50, and 100 mL/min while maintaining the Ar flow rate and process temperature. The obtained samples were

denoted as ahCNF-10, ahCNF-50, and ahCNF-100, where the numbers represent the percentage ratio of the NH$_3$ flow rate to the Ar flow rate. The heating rate for the stabilization and carbonization processes was 5 °C/min. Activated CNF without a hollow structure (aCNF-100) was prepared by electrospinning the PAN solution (12 wt %) with a 25G needle and carbonizing/activating the electrospun fibers with NH$_3$ (100 mL/min) and Ar (100 mL/min).

2.2. Characterization of Materials.
Scanning electron microscopy (SEM, JSM-7600F, Jeol), transmission electron microscopy (TEM, JEM-2100F, Jeol), and Raman spectroscopy (XperRam35 V with a 532 nm wavelength excitation laser, Nanobase) were used to characterize the morphology and structure of the synthesized materials. The chemical structure was investigated by X-ray photoelectron spectroscopy (XPS, ESCALAB 250, Thermo Fisher Scientific). The N$_2$ adsorption−desorption isotherms were measured at 77 K (BEL-SORP-mini II, Microtrac) and the SSA was calculated by using the Brunauer−Emmett−Teller (BET) method. The Barrett−Joyner−Halenda (BJH) method was utilized to evaluate the pore size distributions and pore volumes.

2.3. Electrochemical Measurements.
The CNF-based sheets, without any binders or conductive additives, were cut into pieces of a 1 × 1 cm area with a mass loading of at least 1 mg as freestanding electrodes for symmetric supercapacitors. A symmetric two-electrode system was assembled for a supercapacitor test cell using two identical CNF electrodes, two current collectors (conductive polymer film, 2267p, z-flo), a separator (3501, Celgard), and a 6 M KOH aqueous electrolyte.

A flexible supercapacitor was fabricated by using a gel electrolyte. A gel electrolyte was prepared by dissolving poly(vinyl alcohol) (PVA) (1 g, M_w = 89,000−98,000, Merck) and H$_3$PO$_4$ (1 g, 85 wt %, Merck) in 10 mL of DI water at 90 °C. Ti foil as a current collector and a CNF electrode were placed on a flexible polyethylene terephthalate (PET) film and connected using Ag paste. The PVA/H$_3$PO$_4$ gel electrolyte was poured into the active area of the CNF electrodes and dried at room temperature. Two electrodes with the PET films were assembled for a flexible supercapacitor.

The electrochemical performance of the fabricated devices was evaluated by conducting cyclic voltammetry (CV), galvanostatic charge/discharge (GCD), and electrochemical impedance spectroscopy (EIS) using a potentiostat (Autolab PGSTAT204, Metrohm). Electrochemical tests, including CV and GCD, of CNF-based electrodes were carried out in the operating voltage range of 0−1 V.

The specific capacitance of a single electrode (C_{sp}) is calculated from the GCD discharge curves using the following equation[41]

$$C_{sp} = \frac{2I}{m(dV/dt)}$$

where I (A) is the discharge current, m (g) is the mass of the single electrode, and dV/dt (V/s) is obtained from the slope of the discharge curve.

The specific capacitance (C_{sp}) is also estimated from the CV curves using the following equation[42]
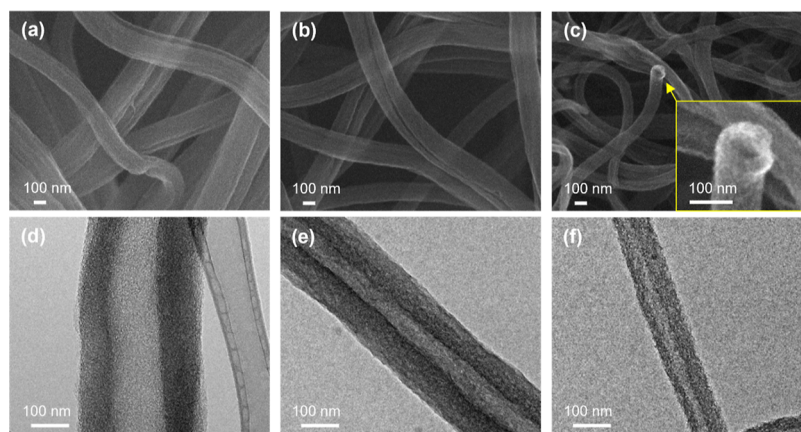
$$C_{sp} = \frac{2 \int I \, dV}{v \Delta V m}$$

Figure 1. Morphology of ahCNFs. SEM images of (a) ahCNF-10, (b) ahCNF-50, and (c) ahCNF-100. The inset of (c) shows a high-magnification SEM image. TEM images of (d) ahCNF-10, (e) ahCNF-50, and (f) ahCNF-100.
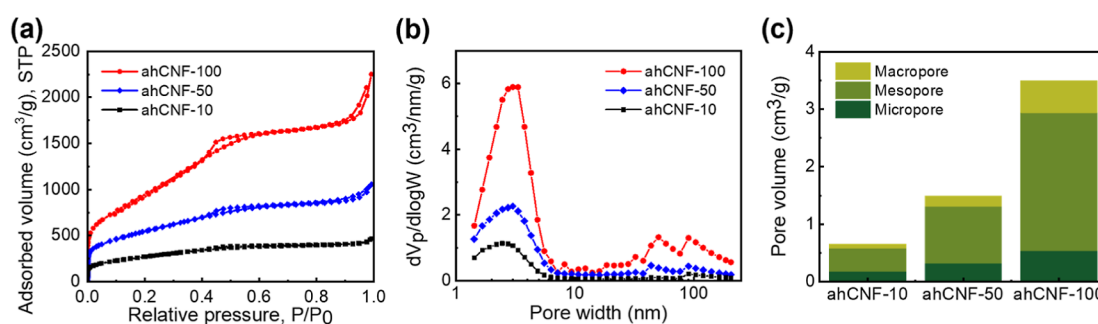

Figure 2. Pore characteristics of ahCNFs. (a) N_2 adsorption−desorption isotherms. (b) Pore size distributions. (c) Calculated pore volumes estimated by the BJH method.

where I (A) is the current, V (V) is the voltage, v (V/s) is the scan rate, ΔV (V) is the operating voltage range, and m (g) is the mass of the single electrode.

The energy density (E) and power density (P) of symmetric supercapacitors were calculated according to the following equations, respectively[42]

$$E = \frac{1}{8}C_{sp}V^2$$

$$P = \frac{E}{\Delta t}$$

where V (V) is the voltage range and Δt (s) is the discharge time.

3. RESULTS AND DISCUSSION

3.1. Synthesis of Activated Hollow Carbon Nanofibers.
The electrospinning and carbonization/activation process produced interconnected, uniform, and continuous fiber networks for all samples, including PMMA/PAN nanofibers (Figure S1a), ahCNFs (Figure 1a−c), and aCNFs (Figure S2a). Compared to PMMA/PAN nanofibers (Figure S1a,b), SEM observation shows that ahCNFs and aCNFs have a rough surface morphology due to NH_3 etching and activation (Figures 1a−c and S2a,b). TEM images clearly show the hollow structures of ahCNFs (Figure 1d−f) generated by the thermal decomposition of PMMA during the carbonization process, while aCNFs possessed solid and full-filled fiber structures (Figure S2c). The presence of hollow structures facilitates the diffusion of NH_3 gas to the CNF surfaces during

the activation process. Furthermore, they enhance the charge storage area and promote ion diffusion, which significantly benefits the supercapacitor performance.[43]

As the NH_3 concentration increased, the average diameter of ahCNFs decreased to about 280, 220, and 120 nm for ahCNF-10, -50, and -100, respectively. The average inner core diameter of ahCNFs was reduced to about 75, 55, and 45 nm for ahCNF-10, -50, and -100, respectively. The decrease in the outer and inner core diameters of ahCNFs is attributed to the strong etching of carbonized fiber structures by NH_3, which helps to enhance the SSA.[33] It has been known that NH_3 decomposes to active radicals such as atomic H, NH, and NH_2 at high temperatures, and these radicals etch the surface carbon atoms by reacting with carbon and producing carbon-containing species such as methane and hydrogen cyanide.[44−46] More specifically, NH_3 gas reacts with carbon atoms and leads to gasification through the following reaction at high temperatures above 700 °C: $C + NH_3 \rightarrow HCN + H_2$.[47,48] Based on this etching mechanism, carbon atoms are partially eliminated from CNFs, resulting in the formation of micro- and mesoporous structures.[30,49]

3.2. Pore Structures and Nitrogen Doping of ahCNFs.
The pore structures of ahCNFs were investigated by N_2 adsorption−desorption measurements. The N_2 adsorption−desorption isotherms of ahCNFs exhibited a type IV characteristic with a hysteresis loop, in accordance with the International Union of Pure and Applied Chemistry (IUPAC) classification, indicating the presence of mesoporous structures (Figure 2a).[25,50] The SSA values were calculated using the BET method in the P/P_0 range of 0.1−0.3. The SSA values
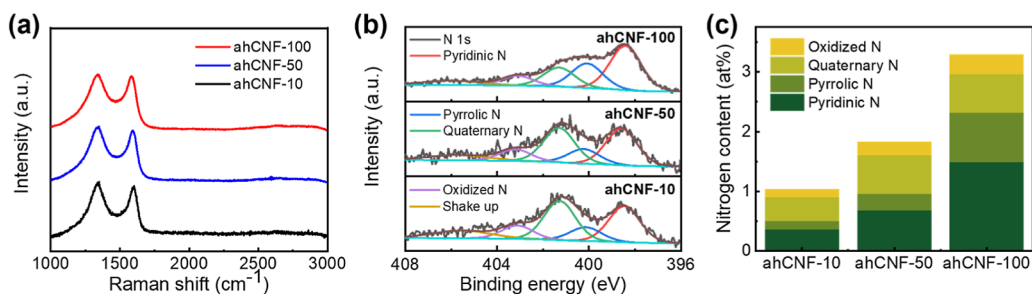
Figure 3. Structural and chemical analyses of ahCNFs. (a) Raman spectra. (b) XPS N 1s spectra. (c) Nitrogen functional group contents estimated from XPS N 1s spectra.
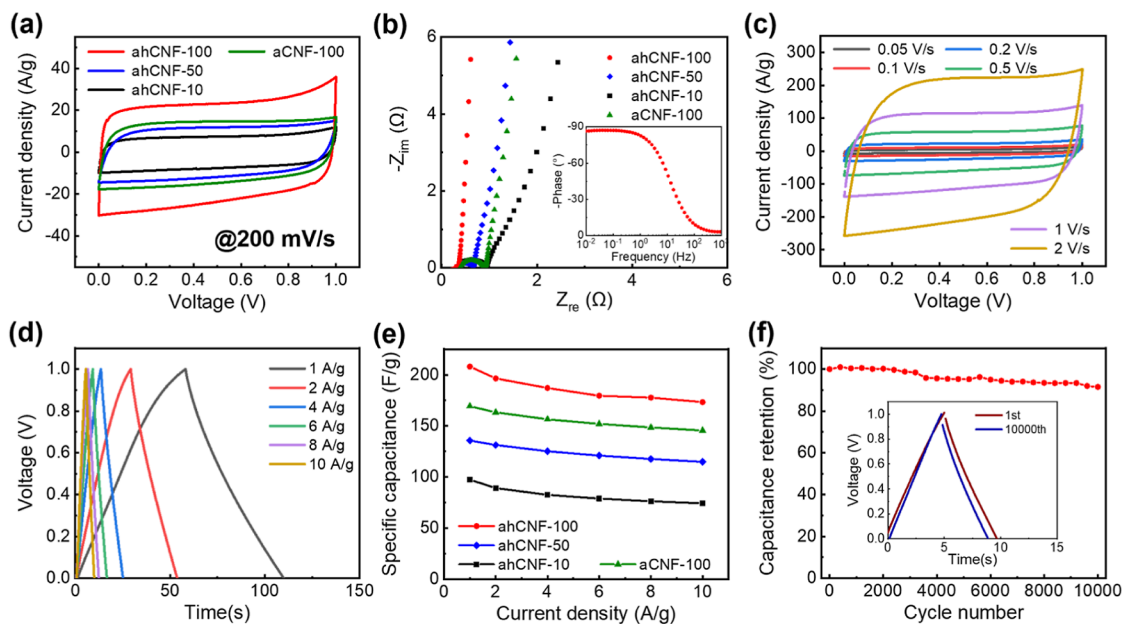

Figure 4. (a) CV curves at a scan rate of 200 mV/s and (b) Nyquist plot of ahCNFs and aCNF in a 6 M KOH aqueous electrolyte. The inset of (b) shows a Bode plot of ahCNF-100. (c) CV curves at different scan rates and (d) GCD curves at different current densities of ahCNF-100. (e) Specific capacitance of ahCNFs and aCNF obtained from GCD curves at different current densities. (f) Cyclic stability of ahCNF-100 at a current density of 10 A/g. The inset of (f) shows GCD curves of the 1st and 10,000th cycles.

were 972, 1947, and 3618 m^2/g for ahCNF-10, -50, and -100, respectively. The SSA value of ahCNF-100 is much higher than the theoretical SSA value of graphene (∼2630 m^2/g). Figures 2b and S3 show the pore size distribution of ahCNFs estimated by the BJH method and nonlocal density functional theory (NLDFT) method, respectively. The ahCNFs possessed large amounts of mesopores with sizes smaller than 5 nm as well as macropores with dimensions in tens of nanometers. The mesopores were formed by the activation process with NH$_3$, while the macropores were a result of the hollow core structures of the fibers and etching effects. Figure 2c delineates the total pore volume and ratios of micro-, meso-, and macropores in ahCNFs calculated by the BJH method. The total pore volume increased to 0.65, 1.49, and 3.50 cm^3/g for ahCNF-10, -50, and -100, respectively, with increasing the NH$_3$ concentration. Furthermore, the volume ratio of mesopores increased from 62.0 for ahCNF-10 to 66.5 and 68.6% for ahCNF-50 and -100, respectively, while that of micropores decreased from 27.7 for ahCNF-10 to 12.0 and 15.4% for ahCNF-50 and -100, respectively. As the mesopores are desirable for fast electrolyte ion diffusion and abundant charge adsorption sites,[51] the core–shell structure with the

NH$_3$ activation is a promising method to develop the mesopores for high-performance supercapacitors.

Raman spectroscopy of ahCNFs shows the D band at ∼1345 cm^{-1} and the G band at ∼1590 cm^{-1} (Figure 3a). The peak intensity ratios of the D to G bands (I_D/I_G), which provide an indication of the degree of disordered carbons,[52] were 1.08, 1.11, and 1.15 for ahCNF-10, -50, and -100, respectively. This implies that the NH$_3$ activation process induces more defects in the carbonized structures. The chemical characteristics of ahCNFs were investigated using XPS. The XPS N 1s spectra were deconvoluted with five spectral components: pyridinic N (N-6) at 398.6 eV, pyrrolic N (N-5) at 400.2 eV, quaternary-N (N-Q) at 401.3 eV, oxidized-N at 403.2 eV, and shakeup satellites at 405.5 eV (Figure 3b).[53] The N-6 and N-5 species mainly contribute to the pseudocapacitive reactions, which can enhance the charge storage capability.[54] The total nitrogen atomic percentages of ahCNFs were 1.18, 2.01, and 3.56% for ahCNF-10, -50, and -100, respectively (Figures 3c, S4, and Table S1). The proportions of N-6 and N-5 of ahCNFs significantly increased to 41.92 and 23.22%, respectively, with an increase in the NH$_3$ concentration, while the proportion of N-Q decreased to 18.06%. The detailed chemical analysis revealed that NH$_3$ activation at high temperatures induced

more nitrogen doping in the CNFs in the form of electrochemically active species.

3.3. Electrochemical Performances of ahCNFs.

The electrochemical performances of ahCNFs and aCNF were evaluated by using a symmetric two-electrode configuration with a 6 M KOH aqueous electrolyte. The CV curves of ahCNF-10, -50, -100, and aCNF-100 at a scan rate of 200 mV/s show nearly rectangular shapes (Figure 4a), indicating dominant EDLC behaviors. The small distortion of the CV curves implies potential pseudocapacitive behaviors caused by the nitrogen functional groups of the activated samples. The ahCNF-100 exhibited the largest closed area in the CV curve, which is proportional to its specific capacitance. Figure 4b shows the Nyquist plots of all samples at frequencies ranging from 500 kHz to 0.01 Hz. The real axis intercept in the high-frequency region is related to the electrolyte, electrode, current collector, and their contact resistances.[55,56] The ahCNFs and aCNF showed almost similar real axis intercepts at 0.3−0.4 Ω. The charge transfer resistance, represented by the diameter of a semicircle in the high-frequency region, is associated with the electrode/electrolyte interface and the movement of electrolyte ions within the pore structures of electrodes.[36,56,57] The charge transfer resistances of ahCNF-10, -50, -100, and aCNF-100 were 0.6, 0.3, 0.02, and 0.5 Ω, respectively, indicating that ahCNF-100 exhibited a fast charge transfer mechanism. The plot of ahCNF-100 in the low-frequency region is close to a vertical curve, indicating nearly ideal capacitive behavior.[58] Furthermore, the capacitive behavior of ahCNF-100 is confirmed by the phase angle, which is nearly −90° at low frequencies in the Bode plot, as shown in the inset of Figure 4b.[59]

Figure 4c,d show the CV and GCD curves of the ahCNF-100 electrode under various conditions. The CV curves showed that ahCNF-100 retained a nearly rectangular shape, even at a high scan rate of 2 V/s (Figure 4c). The GCD curves at various current densities had symmetric shapes with a small voltage (IR) drop at the beginning of the discharge (Figure 4d). The small IR drop is associated with a small equivalent series resistance (ESR) of the device, as analyzed by the Nyquist plot. The specific capacitances calculated from discharge curves at a current density of 1 A/g were 97, 136, 208, and 170 F/g for ahCNF-10, -50, -100, and aCNF-100, respectively. The ahCNF-100 electrode exhibits the highest specific capacitance due to its superior SSA and nitrogen content. Moreover, the specific capacitance of ahCNF-100 was higher than that of aCNF-100, implying that the hollow structures of the fiber were effective in improving the electrochemical storage capability. Figure 4e shows the specific capacitance change with increasing current density. The capacitance of ahCNF-100 tested at 10 A/g remained at 83% of the capacitance at 1 A/g, showing a good rate capability. The cyclic stability was evaluated by the GCD tests over 10,000 cycles at a current density of 10 A/g (Figure 4f). The supercapacitor with the ahCNF-100 electrodes exhibited a capacitance retention of 91.5% from the initial capacitance value even after 10,000 cycles.

Furthermore, the supercapacitor fabricated with ahCNF-100 was subjected to a floating voltage test, which is regarded as a reliable way for determining long-term stability and appropriate maximum operating voltage, at a voltage load of 1 V for 100 h.[60,61] Figure S5 displays the changes in specific capacitance and Coulombic efficiency as well as ESR of ahCNF-100 over the floating time. After 100 h of floating time, the specific capacitance of ahCNF-100 decreased by 16.2%, while the ESR of ahCNF-100 increased by 79.1%. Considering the reported criteria for end-of-life of supercapacitor devices (capacitance loss of 20%), the ahCNF-100 exhibits adequate long-term stability over 100 h of the floating voltage test.[62,63] In addition, the Coulombic efficiency of ahCNF-100 was about 94% after 100 h of the floating voltage test, indicating good electrochemical reversibility.[64]

The electrochemical performance of ahCNF-100 in acidic, neutral, and alkaline aqueous electrolytes was evaluated using 1 M H_2SO_4, 1 M Li_2SO_4, and 6 M KOH, respectively. Figure S6a shows the CV curves of supercapacitors using ahCNF-100 at a scan rate of 200 mV/s. The operating potential ranges in 1 M H_2SO_4, 1 M Li_2SO_4, and 6 M KOH were 1, 1.8, and 1 V, respectively (Figure S6). The specific capacitances obtained from the GCD curves at a current density of 1 A/g in 1 M H_2SO_4, 1 M Li_2SO_4, and 6 M KOH were 170, 144, and 208 F/g, respectively.

The symmetric supercapacitor using the ahCNF-100 electrodes in 6 M KOH electrolyte showed an energy density of 7.22 W h/kg at a power density of 502 W/kg and a power density of 5.12 kW/kg at an energy density of 6.02 W h/kg, which are competitive with those of typical commercial supercapacitors.[65,66] In addition, the supercapacitor using the ahCNF-100 electrodes in 1 M Li_2SO_4 neutral electrolyte achieved 16.17 W h/kg at a power density of 902.6 W/kg due to the wide operating voltage range of 1.8 V. Table S2 compares the electrochemical performance of the ahCNF-100 electrode with other previously reported works. The ahCNF-100 electrode surpasses the performances of most PAN-based porous CNF materials, including porous nitrogen-doped CNFs synthesized from PAN/PVP (148 F/g),[35] KOH activated CNFs (191 F/g),[67] H_3PO_4 activated CNFs (156 F/g),[68] and nitrogen-doped porous hollow CNFs obtained from PAN/PVP shell and poly(styrene-co-acrylonitrile) (SAN) core structures (152 F/g).[36] This can be ascribed to the exceptionally high SSA of ahCNF-100 obtained by NH_3 activation with the help of the hollow structure. In addition, nitrogen doping by the NH_3 treatment could help to enhance the electrochemical performance of ahCNF-100.

A flexible supercapacitor was fabricated using the free-standing, binder-free ahCNF-100 electrode with a PVA/H_3PO_4 gel electrolyte. The CV curves of the flexible supercapacitor at scan rates of 10 and 20 mV/s display quasi-rectangular shapes (Figure 5a). The specific capacitance of the device was 136 F/g at 10 mV/s. The Nyquist plot of the flexible supercapacitor obtained by the EIS measurement shows a small charge transfer resistance in the high-frequency region and a nearly vertical curve in the low-frequency region (Figure S7). Because the freestanding ahCNF electrode is mechanically robust and flexible, the supercapacitor can be bent at various bending angles by using a linear motion guide, as shown in Figure 5b. The electrochemical performance of the device was measured at bending angles of 0, 70, and 140°. Figure 5c shows that the CV curves obtained at different bending angles are nearly identical. Moreover, the capacitance of the device was measured while the device was bent 500 times at a bending angle of 140° (Figure 5d). After 500 bending cycles, the capacitance was 96% of the initial capacitance. These results demonstrate the great potential of the ahCNF electrode for high-performance, flexible energy storage devices.
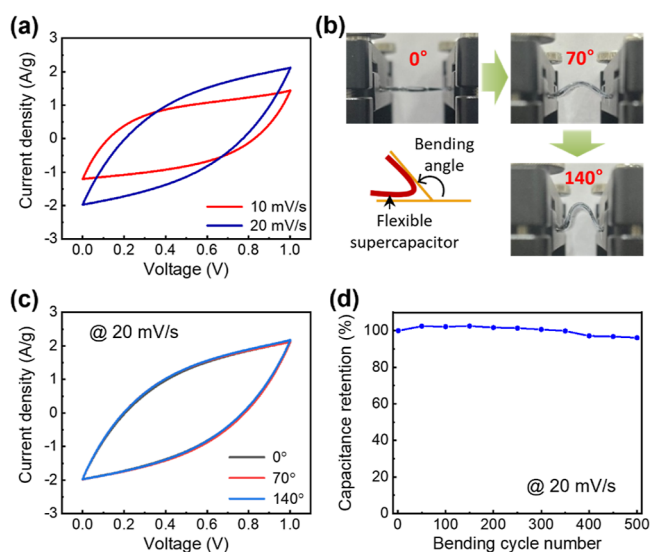
Figure 5. Flexible supercapacitor using ahCNF-100 electrodes. (a) CV curves at different scan rates. (b) Photographs of the fabricated flexible supercapacitor at different bending angles. (c) CV curves at different bending angles with a scan rate of 20 mV/s. (d) Capacitance retention over 500 bending cycles at a scan rate of 20 mV/s and a bending angle of 140°.

4. CONCLUSIONS

Nitrogen-doped hollow CNFs with an exceptional SSA were prepared by coaxial electrospinning of PMMA/PAN nanofibers and their carbonization and activation under NH_3. Heat treatments with a high-concentration NH_3 gas developed mesoporous structures with a large pore volume and induced nitrogen doping. The hollow inner structure of ahCNFs was derived from the pyrolysis of the PMMA core during the carbonization, which was beneficial for facilitating the activation of CNFs and improving ion diffusion and charge storage capability of supercapacitors. Therefore, the ahCNF-100 showed high electrochemical performances with a high specific capacitance of 208 F/g at 1 A/g, good rate capability (83% retention at 10 A/g compared to capacitance at 1 A/g), and good cyclic stability (91.5% retention after 10,000 cycles) in a 6 M KOH aqueous electrolyte. Because the ahCNF-100 sheet was freestanding and mechanically flexible, it was used as a binder-free electrode for a flexible supercapacitor with a PVA/H_3PO_4 gel electrolyte. This work provides the great potential of NH_3-based carbonization/activation on core−shell nanofibers and the resulting ahCNF electrodes for high-performance energy storage devices.

■ ASSOCIATED CONTENT

ⓢ Supporting Information

The Supporting Information is available free of charge at https://pubs.acs.org/doi/10.1021/acsomega.3c08952.

Floating voltage tests, SEM images and XPS survey spectra of nanofibers, pore size distributions, nitrogen atomic contents of nanofibers, electrochemical performances using different electrolytes, comparison of SSAs and specific capacitances of CNF-based electrodes, and Nyquist plot of a flexible supercapacitor (PDF)

■ AUTHOR INFORMATION

Corresponding Author

Ji Won Suk − *School of Mechanical Engineering, Sungkyunkwan University, Suwon, Gyeonggi-do 16419, Republic of Korea; Department of Smart Fab. Technology and SKKU Advanced Institute of Nanotechnology (SAINT), Sungkyunkwan University, Suwon, Gyeonggi-do 16419, Republic of Korea;* ⓞ orcid.org/0000-0002-3953-6617; Phone: +82-31-290-7469; Email: jwsuk@skku.edu

Authors

TaeGyeong Lim − *School of Mechanical Engineering, Sungkyunkwan University, Suwon, Gyeonggi-do 16419, Republic of Korea*

Bong Hyun Seo − *School of Mechanical Engineering, Sungkyunkwan University, Suwon, Gyeonggi-do 16419, Republic of Korea*

Seo Ju Kim − *School of Mechanical Engineering, Sungkyunkwan University, Suwon, Gyeonggi-do 16419, Republic of Korea*

Seungwoo Han − *School of Mechanical Engineering, Sungkyunkwan University, Suwon, Gyeonggi-do 16419, Republic of Korea*

Wonyoung Lee − *School of Mechanical Engineering, Sungkyunkwan University, Suwon, Gyeonggi-do 16419, Republic of Korea; SKKU Institute of Energy Science and Technology (SIEST), Sungkyunkwan University, Suwon, Gyeonggi-do 16419, Republic of Korea;* ⓞ orcid.org/0000-0002-1349-4017

Complete contact information is available at:
https://pubs.acs.org/10.1021/acsomega.3c08952

Notes

The authors declare no competing financial interest.

■ REFERENCES

(1) Liu, Z.; Lu, T.; Song, T.; Yu, X.-Y.; Lou, X. W. D.; Paik, U. Structure-designed synthesis of FeS 2@ C yolk-shell nanoboxes as a high-performance anode for sodium-ion batteries. *Energy Environ. Sci.* **2017**, *10* (7), 1576−1580.

(2) Yang, Z.; Tian, J.; Yin, Z.; Cui, C.; Qian, W.; Wei, F. Carbon nanotube-and graphene-based nanomaterials and applications in high-voltage supercapacitor: A review. *Carbon* **2019**, *141*, 467−480.

(3) Heo, Y.-J.; Lee, H. I.; Lee, J. W.; Park, M.; Rhee, K. Y.; Park, S.-J. Optimization of the pore structure of PAN-based carbon fibers for enhanced supercapacitor performances via electrospinning. *Composites, Part B* **2019**, *161*, 10−17.

(4) Stoller, M. D.; Park, S.; Zhu, Y.; An, J.; Ruoff, R. S. Graphene-based ultracapacitors. *Nano Lett.* **2008**, *8* (10), 3498−3502.

(5) Dai, P.; Zhang, S.; Liu, H.; Yan, L.; Gu, X.; Li, L.; Liu, D.; Zhao, X. Cotton fabrics-derived flexible nitrogen-doped activated carbon cloth for high-performance supercapacitors in organic electrolyte. *Electrochim. Acta* **2020**, *354*, 136717.

(6) Wang, K.; Song, Y.; Yan, R.; Zhao, N.; Tian, X.; Li, X.; Guo, Q.; Liu, Z. High capacitive performance of hollow activated carbon fibers derived from willow catkins. *Appl. Surf. Sci.* **2017**, *394*, 569−577.

(7) Zhang, L. L.; Zhao, X. Carbon-based materials as supercapacitor electrodes. *Chem. Soc. Rev.* **2009**, *38* (9), 2520−2531.

(8) Xu, C.; Xu, B.; Gu, Y.; Xiong, Z.; Sun, J.; Zhao, X. Graphene-based electrodes for electrochemical energy storage. *Energy Environ. Sci.* **2013**, *6* (5), 1388−1414.

(9) Yin, J.; Zhang, W.; Alhebshi, N. A.; Salah, N.; Alshareef, H. N. Synthesis strategies of porous carbon for supercapacitor applications. *Small Methods* **2020**, *4* (3), 1900853.

(10) Hwang, Y.-H.; Lee, S. M.; Kim, Y. J.; Kahng, Y. H.; Lee, K. A new approach of structural and chemical modification on graphene electrodes for high-performance supercapacitors. *Carbon* **2016**, *100*, 7−15.

(11) Najib, S.; Erdem, E. Current progress achieved in novel materials for supercapacitor electrodes: mini review. *Nanoscale Adv.* **2019**, *1* (8), 2817−2827.

(12) Kim, T.; Jung, G.; Yoo, S.; Suh, K. S.; Ruoff, R. S. Activated graphene-based carbons as supercapacitor electrodes with macro-and mesopores. *ACS Nano* **2013**, *7* (8), 6899−6905.

(13) Zheng, X.; Luo, J.; Lv, W.; Wang, D. W.; Yang, Q. H. Two-dimensional porous carbon: Synthesis and ion-transport properties. *Adv. Mater.* **2015**, *27* (36), 5388−5395.

(14) Zhang, W.; Cheng, R.-r.; Bi, H.-h.; Lu, Y.-h.; Ma, L.-b.; He, X.-j. A review of porous carbons produced by template methods for supercapacitor applications. *New Carbon Mater.* **2021**, *36* (1), 69−81.

(15) Wang, K.; Wang, Y.; Wang, Y.; Hosono, E.; Zhou, H. Mesoporous carbon nanofibers for supercapacitor application. *J. Phys. Chem. C* **2009**, *113* (3), 1093−1097.

(16) Ahmad, M. W.; Anand, S.; Dey, B.; Fatima, A.; Yang, D. J.; Choudhury, A. N/P/O/S heteroatom-doped porous carbon nanofiber mats derived from a polyacrylonitrile/l-cysteine/P2O5 precursor for flexible electrochemical supercapacitors. *ACS Appl. Energy Mater.* **2021**, *4* (11), 12177−12190.

(17) Ahmad, M. W.; Anand, S.; Dey, B.; Yang, D.-J.; Choudhury, A. Asymmetric supercapacitors based on porous MnMoS4 nanosheets-anchored carbon nanofiber and N, S-doped carbon nanofiber electrodes. *J. Alloys Compd.* **2022**, *906*, 164271.

(18) Ahmad, M. W.; Anand, S.; Shalini, K.; Ul-Islam, M.; Yang, D.-J.; Choudhury, A. MnMoO4 nanorods-encapsulated carbon nanofibers hybrid mat as binder-free electrode for flexible asymmetric super-capacitors. *Mater. Sci. Semicond. Process.* **2021**, *136*, 106176.

(19) Anand, S.; Choudhury, A. MnMoS4 anchored at carbon nanofiber as a flexible electrode for solid-state asymmetric super-capacitor device. *Mater. Chem. Phys.* **2023**, *299*, 127517.

(20) Kim, C.; Jeong, Y. I.; Ngoc, B. T. N.; Yang, K. S.; Kojima, M.; Kim, Y. A.; Endo, M.; Lee, J. W. Synthesis and characterization of porous carbon nanofibers with hollow cores through the thermal treatment of electrospun copolymeric nanofiber webs. *Small* **2007**, *3* (1), 91−95.

(21) Li, Y.; Zhu, J.; Cheng, H.; Li, G.; Cho, H.; Jiang, M.; Gao, Q.; Zhang, X. Developments of advanced electrospinning techniques: A critical review. *Adv. Mater. Technol.* **2021**, *6* (11), 2100410.

(22) Jang, J.; Bae, J.; Choi, M.; Yoon, S.-H. Fabrication and characterization of polyaniline coated carbon nanofiber for super-capacitor. *Carbon* **2005**, *43* (13), 2730−2736.

(23) Anand, S.; Ahmad, M. W.; Fatima, A.; Kumar, A.; Bharadwaj, A.; Yang, D.-J.; Choudhury, A. Flexible nickel disulfide nanoparticles-anchored carbon nanofiber hybrid mat as a flexible binder-free cathode for solid-state asymmetric supercapacitors. *Nanotechnology* **2021**, *32* (49), 495403.

(24) Choudhury, A.; Dey, B.; Mahapatra, S. S.; Kim, D.-W.; Yang, K.-S.; Yang, D.-J. Flexible and freestanding supercapacitor based on nanostructured poly (m-aminophenol)/carbon nanofiber hybrid mats with high energy and power densities. *Nanotechnology* **2018**, *29* (16), 165401.

(25) Zhu, Y.; Murali, S.; Stoller, M. D.; Ganesh, K. J.; Cai, W.; Ferreira, P. J.; Pirkle, A.; Wallace, R. M.; Cychosz, K. A.; Thommes, M.; et al. Carbon-based supercapacitors produced by activation of graphene. *Science* **2011**, *332* (6037), 1537−1541.

(26) Xu, Q.; Yu, X.; Liang, Q.; Bai, Y.; Huang, Z.-H.; Kang, F. Nitrogen-doped hollow activated carbon nanofibers as high perform-ance supercapacitor electrodes. *J. Electroanal. Chem.* **2015**, *739*, 84−88.

(27) Lim, T.; Ho, B. T.; Suk, J. W. High-performance and thermostable wire supercapacitors using mesoporous activated graphene deposited on continuous multilayer graphene. *J. Mater. Chem. A* **2021**, *9* (8), 4800−4809.

(28) Ho, B. T.; Lim, T.; Jeong, M. H.; Suk, J. W. Graphene fibers containing activated graphene for high-performance solid-state flexible supercapacitors. *ACS Appl. Energy Mater.* **2021**, *4* (9), 8883−8890.

(29) Lim, T.; Suk, J. W. Effect of the particle size of graphene oxide powders on the electrochemical performance of graphene-based supercapacitors. *Funct. Compos. Struct.* **2021**, *3* (1), 015005.

(30) Wang, J.; Kaskel, S. KOH activation of carbon-based materials for energy storage. *J. Mater. Chem.* **2012**, *22* (45), 23710−23725.

(31) Williams, N. E.; Oba, O. A.; Aydinlik, N. P. Modification, Production, and Methods of KOH-Activated Carbon. *ChemBioEng Rev.* **2022**, *9* (2), 164−189.

(32) Qiu, Y.; Yu, J.; Shi, T.; Zhou, X.; Bai, X.; Huang, J. Y. Nitrogen-doped ultrathin carbon nanofibers derived from electrospinning: Large-scale production, unique structure, and application as electro-catalysts for oxygen reduction. *J. Power Sources* **2011**, *196* (23), 9862−9867.

(33) Zhao, L.; Qiu, Y.; Yu, J.; Deng, X.; Dai, C.; Bai, X. Carbon nanofibers with radially grown graphene sheets derived from electrospinning for aqueous supercapacitors with high working voltage and energy density. *Nanoscale* **2013**, *5* (11), 4902−4909.

(34) Wu, D.; Li, Z.; Zhong, M.; Kowalewski, T.; Matyjaszewski, K. Templated synthesis of nitrogen-enriched nanoporous carbon materials from porogenic organic precursors prepared by ATRP. *Angew. Chem., Int. Ed.* **2014**, *53* (15), 3957−3960.

(35) Li, X.; Zhao, Y.; Bai, Y.; Zhao, X.; Wang, R.; Huang, Y.; Liang, Q.; Huang, Z. A non-woven network of porous nitrogen-doping carbon nanofibers as a binder-free electrode for supercapacitors. *Electrochim. Acta* **2017**, *230*, 445−453.

(36) Kim, J.-G.; Kim, H.-C.; Kim, N. D.; Khil, M.-S. N-doped hierarchical porous hollow carbon nanofibers based on PAN/PVP@ SAN structure for high performance supercapacitor. *Composites, Part B* **2020**, *186*, 107825.

(37) Lv, J.; Gu, W.; Cui, X.; Dai, S.; Zhang, B.; Ji, G. Nanofiber network with adjustable nanostructure controlled by PVP content for an excellent microwave absorption. *Sci. Rep.* **2019**, *9* (1), 4271.

(38) Poolakkandy, R. R.; Menamparambath, M. M. Soft-template-assisted synthesis: a promising approach for the fabrication of transition metal oxides. *Nanoscale Adv.* **2020**, *2* (11), 5015−5045.

(39) Gopalakrishnan, A.; Sahatiya, P.; Badhulika, S. Template-assisted electrospinning of bubbled carbon nanofibers as binder-free electrodes for high-performance supercapacitors. *ChemElectroChem* **2018**, *5* (3), 531−539.

(40) Shilpa, S.; Sharma, A. Free standing hollow carbon nanofiber mats for supercapacitor electrodes. *RSC Adv.* **2016**, *6* (82), 78528−78537.

(41) Zhang, L. L.; Zhao, X.; Stoller, M. D.; Zhu, Y.; Ji, H.; Murali, S.; Wu, Y.; Perales, S.; Clevenger, B.; Ruoff, R. S. Highly conductive and porous activated reduced graphene oxide films for high-power supercapacitors. *Nano Lett.* **2012**, *12* (4), 1806−1812.

(42) Chee, W.; Lim, H.; Zainal, Z.; Huang, N.; Harrison, I.; Andou, Y. Flexible graphene-based supercapacitors: a review. *J. Phys. Chem. C* **2016**, *120* (8), 4153−4172.

(43) Chen, L.-F.; Lu, Y.; Yu, L.; Lou, X. W. D. Designed formation of hollow particle-based nitrogen-doped carbon nanofibers for high-performance supercapacitors. *Energy Environ. Sci.* **2017**, *10* (8), 1777−1783.

(44) Stöhr, B.; Boehm, H.; Schlögl, R. Enhancement of the catalytic activity of activated carbons in oxidation reactions by thermal treatment with ammonia or hydrogen cyanide and observation of a superoxide species as a possible intermediate. *Carbon* **1991**, *29* (6), 707−720.

(45) Wang, M.-X.; Guo, Z.; Huang, Z.-H.; Kang, F. NH3-activated carbon nanofibers for low-concentration NO removal at room temperature. *Catal. Commun.* **2015**, *62*, 83−88.

(46) Mahurin, S. M.; Lee, J. S.; Wang, X.; Dai, S. Ammonia-activated mesoporous carbon membranes for gas separations. *J. Membr. Sci.* **2011**, *368* (1−2), 41−47.

(47) Van Dijen, F.; Pluijmakers, J. The removal of carbon or carbon residues from ceramic powders or greenware with ammonia. *J. Eur. Ceram. Soc.* **1989**, *5* (6), 385−390.

(48) Chollon, G. The high temperature reaction of ammonia with carbon and SiC-C ceramics. *J. Eur. Ceram. Soc.* **2021**, *41* (1), 136−147.

(49) Jiang, L.; Fan, Z. Design of advanced porous graphene materials: from graphene nanomesh to 3D architectures. *Nanoscale* **2014**, *6* (4), 1922−1945.

(50) Sing, K. S. Reporting physisorption data for gas/solid systems with special reference to the determination of surface area and porosity (Recommendations 1984). *Pure Appl. Chem.* **1985**, *57* (4), 603−619.

(51) Xia, K.; Gao, Q.; Jiang, J.; Hu, J. Hierarchical porous carbons with controlled micropores and mesopores for supercapacitor electrode materials. *Carbon* **2008**, *46* (13), 1718−1726.

(52) Díez, N.; Śliwak, A.; Gryglewicz, S.; Grzyb, B.; Gryglewicz, G. Enhanced reduction of graphene oxide by high-pressure hydrothermal treatment. *RSC Adv.* **2015**, *5* (100), 81831−81837.

(53) Figueras, M.; Villar-Garcia, I. J.; Vines, F.; Sousa, C.; de la Peña O'Shea, V. A.; Illas, F. Correcting flaws in the assignment of nitrogen chemical environments in N-doped graphene. *J. Phys. Chem. C* **2019**, *123* (17), 11319−11327.

(54) Zhu, W.; Shen, D.; Xie, H. Combination of chemical activation and nitrogen doping toward hierarchical porous carbon from houttuynia cordata for supercapacitors. *J. Energy Storage* **2023**, *60*, 106595.

(55) Li, B.; Li, Z.; Pang, Q.; Zhuang, Q.; Zhu, J.; Tsiakaras, P.; Shen, P. K. Synthesis and characterization of activated 3D graphene via catalytic growth and chemical activation for electrochemical energy storage in supercapacitors. *Electrochim. Acta* **2019**, *324*, 134878.

(56) Mei, B.-A.; Munteshari, O.; Lau, J.; Dunn, B.; Pilon, L. Physical interpretations of Nyquist plots for EDLC electrodes and devices. *J. Phys. Chem. C* **2018**, *122* (1), 194−206.

(57) Yang, I.; Kim, S.-G.; Kwon, S. H.; Kim, M.-S.; Jung, J. C. Relationships between pore size and charge transfer resistance of carbon aerogels for organic electric double-layer capacitor electrodes. *Electrochim. Acta* **2017**, *223*, 21−30.

(58) Qu, G.; Cheng, J.; Li, X.; Yuan, D.; Chen, P.; Chen, X.; Wang, B.; Peng, H. A fiber supercapacitor with high energy density based on hollow graphene/conducting polymer fiber electrode. *Adv. Mater.* **2016**, *28* (19), 3646−3652.

(59) Bo, Z.; Zhu, W.; Ma, W.; Wen, Z.; Shuai, X.; Chen, J.; Yan, J.; Wang, Z.; Cen, K.; Feng, X. Vertically oriented graphene bridging active-layer/current-collector interface for ultrahigh rate super-capacitors. *Adv. Mater.* **2013**, *25* (40), 5799−5806.

(60) Bello, A.; Barzegar, F.; Madito, M.; Momodu, D. Y.; Khaleed, A. A.; Masikhwa, T.; Dangbegnon, J. K.; Manyala, N. Stability studies of polypyrrole-derived carbon based symmetric supercapacitor via potentiostatic floating test. *Electrochim. Acta* **2016**, *213*, 107−114.

(61) Piwek, J.; Platek, A.; Frackowiak, E.; Fic, K. Mechanisms of the performance fading of carbon-based electrochemical capacitors operating in a LiNO3 electrolyte. *J. Power Sources* **2019**, *438*, 227029.

(62) Keyla, R.-H. I.; Leticia, G.-T. L.; Maximiano, S.-C. E.; Carlos, T.-G. L. Activated carbon from agave wastes (agave tequilana) for supercapacitors via potentiostatic floating test. *J. Mater. Sci.: Mater. Electron.* **2021**, *32*, 21432−21440.

(63) Ratajczak, P.; Jurewicz, K.; Béguin, F. Factors contributing to ageing of high voltage carbon/carbon supercapacitors in salt aqueous electrolyte. *J. Appl. Electrochem.* **2014**, *44*, 475−480.

(64) Akbar, A. R.; Saleem, A.; Rauf, A.; Iqbal, R.; Tahir, M.; Peng, G.; Khan, A. S.; Hussain, A.; Ahmad, M.; Akhtar, M.; et al. Integrated MnO2/PEDOT composite on carbon cloth for advanced electro-chemical energy storage asymmetric supercapacitors. *J. Power Sources* **2023**, *579*, 233181.

(65) Zhao, X.; Sánchez, B. M.; Dobson, P. J.; Grant, P. S. The role of nanomaterials in redox-based supercapacitors for next generation energy storage devices. *Nanoscale* **2011**, *3* (3), 839−855.

(66) Zhou, Z.; Liu, T.; Khan, A. U.; Liu, G. Block copolymer-based porous carbon fibers. *Sci. Adv.* **2019**, *5* (2), No. eaau6852.

(67) Chen, Y.; Amiri, A.; Boyd, J. G.; Naraghi, M. Promising trade-offs between energy storage and load bearing in carbon nanofibers as structural energy storage devices. *Adv. Funct. Mater.* **2019**, *29* (33), 1901425.

(68) Zhi, M.; Liu, S.; Hong, Z.; Wu, N. Electrospun activated carbon nanofibers for supercapacitor electrodes. *RSC Adv.* **2014**, *4* (82), 43619−43623.